Experiment Information Cover Page

Proposal Title: Measurement of the Tensor Analyzing Power in Deuteron Photodisintegration between E_γ = 4 MeV and 20 MeV

Spokesperson-Contact Information:

Name : Pil-Neyo Seo
Email: pilneyo@tunl.duke.edu
Telephone: 919-660-2663

Beam Information

Total Hours of Beam on target: 204

$E_\gamma(MeV)$	Collimator Radius (mm)	Flux on target	Polarization	Hours
4	5	4×10^7	Circular	12
5	5	4×10^7	Circular	12
6	5	4×10^7	Circular	12
7	5	5×10^7	Circular	12
8	5	5×10^7	Circular	12
9	5	6×10^7	Circular	12
10	5	6×10^7	Circular	12
11	5	7×10^7	Circular	12
12	5	8×10^7	Circular	12
13	5	9×10^7	Circular	12
14	5	9×10^7	Circular	12
15	5	1×10^8	Circular	12
16	5	1.1×10^8	Circular	12
17	5	1.2×10^8	Circular	12
18	5	1.3×10^8	Circular	12
19	5	1.4×10^8	Circular	12
20	5	1.5×10^8	Circular	12

Measurement of the Tensor Analyzing Power in Deuteron Photodisintegration between E_γ = 4 MeV and 20 MeV

D. Keller (Spokesperson), H. Chen,D. Crabb, D.B. Day, R. Duve, R. Lindgren, S. Liuti, D. Nguyen, B. Norum (Spokesperson), P. Seo (Spokesperson-Contact), M. Yurov
University of Virginia, Charlottesville, VA 22904

R. Pywell
University of Saskatchewan, Saskatoon, SK, Canada S7N 5E2

D. Higinbotham, B. Sawatzky
Jefferson Lab, Newport News, VA 23606

H. Arenhövel
University of Mainz, 55122 Mainz, Germany

M. Ahmed, C. Howell*, H. Weller*
TUNL, Durham, NC 27708

February 19, 2016

*To be confirmed

1 Experiment Summary

We are proposing to measure the tensor analyzing power $T_{20}\,(\theta_n)$ in deuteron photodisintegration between photon energies of $4\ MeV$ and $20\ MeV$, an energy range not covered in any previous measurement. Several measurements at laboratories around the world over the last 40^{+} years have shown disagreements with our current theoretical descriptions of the deuteron. These include measurements of $d(p,pp)X$ from the Moscow Meson Facility, of $d\,(\vec{\gamma},\pi^{+}\gamma')$ at the LEGS facility at Brookhaven, of $d\,(\gamma,\vec{n})$ at Yale University, of $d(e,e'p)$ TH-Darmstadt, as well as $d\,(\vec{\gamma},n)$ at HIGS. A common feature of these measurements is the indication of a notable discrepancy when the two-nucleon final state has an internal energy of about $9\ MeV$; the measurements at LEGS strongly indicate that this discrepancy has an electric, as opposed to magnetic, origin.

The tensor analyzing power is particularly sensitive to the d-state in the deuteron. In addition, the best current calculations indicate that 1) only the even order terms in the Legendre expansion of $T_{20}\,(\theta_n)$ are expected to contribute significantly; 2) the dominant contribution to the zeroth order term in the Legendre expansion of $T_{20}\,(\theta_n)$ comes from the M1($^1S_0$) amplitude; 3) the second and fourth order terms depend almost completely on electric multipoles. By measuring the angular distribution of $T_{20}\,(\theta_n)$ we will isolate these three terms, the latter two being particularly sensitive to the suggested electric origin of the discrepancies. This will allow us to make unprecedented tests of the best available calculations across this energy range and to further investigate the anomalous behavior near 9 MeV in the residual two-nucleon system.

The measurements will use the fridge of the HIFROST polarized target augmented by a new target cell and related microwave equipment currently under development at UVA. These additions will make possible the tensor polarization of the target while keeping the vector polarization near zero. The Blowfish neutron detector array and the Five-Paddle Beam monitor will also be used. The LUCID-ROOT system will be used for data acquisition.

The measurements will represent the first ever use of a solid, (almost) purely tensor-polarized deuteron target. Not only will it enable us to measure previously unattainable polarization observables, it will provide an excellent opportunity for a graduate student to gain experience with this revolutionary experimental technology.

2 Introduction

The deuteron is the simplest nuclear system and is as important to understanding nuclear forces as the hydrogen atom is to understanding bound systems in QED. However, unlike the case of its atomic analogue, our understanding of the deuteron remains relatively unsatisfying. One of the most fundamental processes that can be studied is the two-body photodisintegration (PD) $\gamma d \rightarrow p + n$. There are many essential observables that have been well studied in the past several decades leading to significant advancement both theoretically and experimentally. However, there are several measurements that show significant deviations from the best available calculations. There are also several observables for which no measurements over critical kinematic ranges are available. Tensor analyzing powers have been measured for photon energies above 40 MeV, but no measurements exist in the important low energy region below 20 MeV, the range accessible using the High Intensity Gamma-Ray Source (HI$\vec{\gamma}$S). The tensor analyzing powers can be accessed using an asymmetry measurement between a tensor polarized target and an unpolarized target. The tensor analyzing powers are unique in that they not only complement the vector asymmetry measurements as additional distinct observables but they give direct information about the correlations between spatial orientation of the nucleons and the scattering mechanism. For example, spatial alignment of the target deuterons can lead to large asymmetries from final state interactions. Building an understanding of the tensor analyzing powers in the HI$\vec{\gamma}$S energy range will also help to interpret effects from short-range correlations at higher energies. Tensor polarization enhances the D-state contribution, which compresses the deuteron, making the system more sensitive to short-range QCD effects. Understanding the nucleon-nucleon potential of the deuteron is essential for understanding short-range correlations as they are largely dependent on the tensor force. A deeper understanding of the deuteron's tensor structure will help to clarify how the gross properties of the nucleus arise from underlying constituents.

A measurement of the photodisintegration tensor analyzing power T_{20} is of considerable interest since it provides a clear and stringent test of the best available nuclear theories. The TUNL HI$\vec{\gamma}$S facility is the only place where it is possible to investigate tensor analyzing powers in a deuteron target in the unmeasured energy range of 4 MeV - 20 MeV. We describe such a measurement in this proposal.

2.1 Background and Motivation

Many measurements of deuteron photodisintegration with photon energies below 20 MeV have shown excellent agreement with calculations. These include total cross section measurements as well as differential cross sections at $\theta_n = 90^o$ [1, 2, 3, 4, 5, 6, 7]. However, even in the latter case discrepancies emerge when one looks deeper. The cross section at $\theta_n = 90^o$ contains contributions from the P_4 as well as the dominant P_2 term. The data of Smit and Brooks[1] obtained at the University of Cape Town, RSA; those of Sawatzky $et\ al.$[2], Blackston $et\ al.$ [3], Kucuker $et\ al.$[4], obtained at HI$\vec{\gamma}$S; as well as those of Skopik $et\ al.$[5] obtained at the Saskatchewan Accelerator Lab combine to show that for photon energies centred on ≈12 MeV the P_2 and P_4 contributions individually disagree with theory but add to yield agreement. These disagreements decrease with increasing photon energy and by $E_\gamma = 20\ MeV$ the disagreement no longer exists.

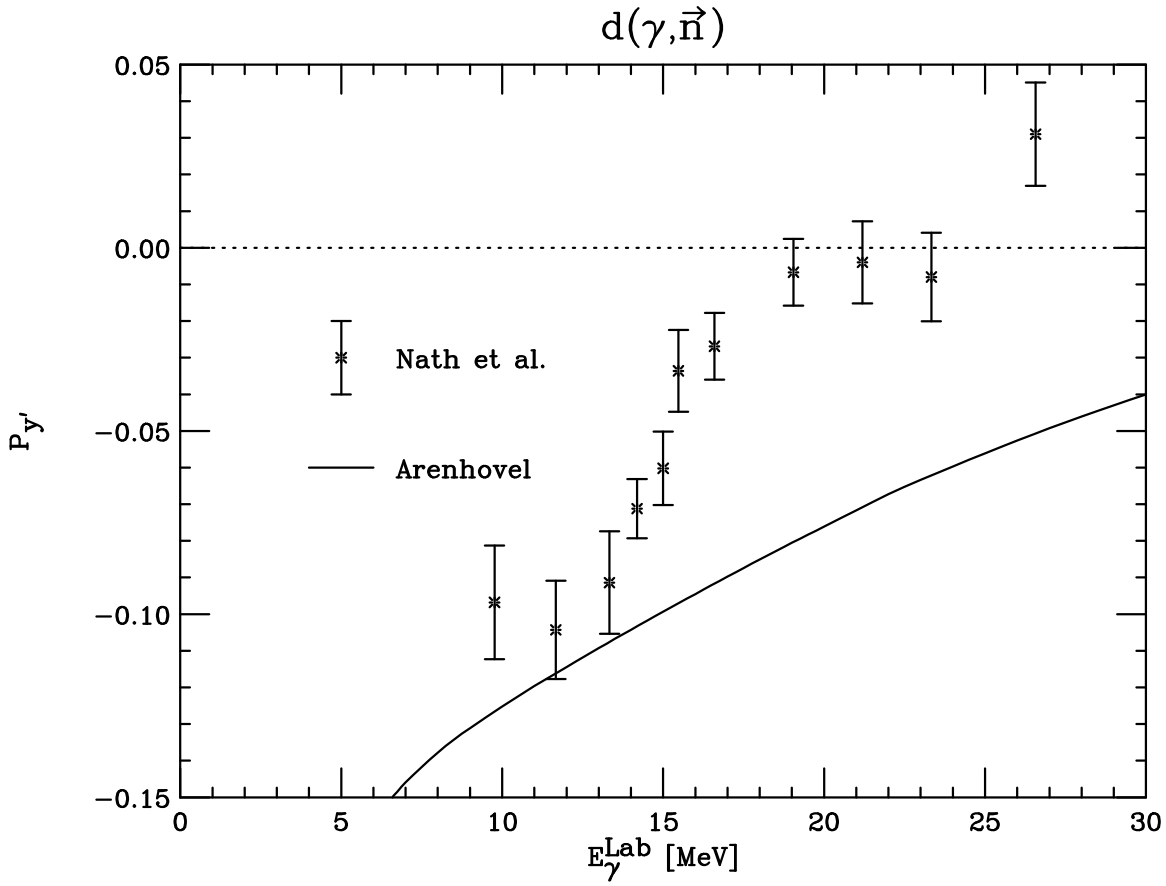

Figure 1: Induced neutron polarization observed by Nath $et\ al.$ [8] at Yale University. The calculation is that of Schmitt and Arenhoevel [10]. Note that a lab frame photon energy of 11-12 MeV corresponds to an internal energy in the final state pn system of about 9 MeV.

More telling, however, are the results of Nath $et\ al.$[8]. Their measurements of the induced neutron polarization in the reaction $d\,(\gamma, \vec{n})$ are shown in Fig. 1 along with the calculation of H. Arenhoevel [9]. The striking departure of the data from the theory at $E_\gamma \approx 11 - 12\ MeV$ has the appearance of a Wigner or Unitary cusp indicating the emergence of another reaction channel with a center-of-mass energy of about 9 MeV above the two-nucleon mass.

The results of Nath are supported by the recent measurements of von Neumann-Cosell $et\ al.$[11] at Darmstadt of near threshold electrodisintegration of deuterium: $d\,(e, e'p)$. Figure 2 shows their result for $\theta_p = 180^o$ compared to the most recent Effective Field Theory calculations (which agree extremely well with the calculations of H. Arenhoevel). Of these results Christlmeier and Griesshammer observed[12], *If the discrepancies were confirmed, this would pose a highly non-trivial problem for nuclear theory.* It is notable that the value of E_x^{lab}, the internal energy of the outgoing pn system in the lab frame, corresponds to approximately $9\ MeV$ in the center-of-mass. This is the energy at which the Nath data diverged from the theory.

Measurements from the Moscow Meson Factory (MMF) [13] and the Laser Electron Gamma

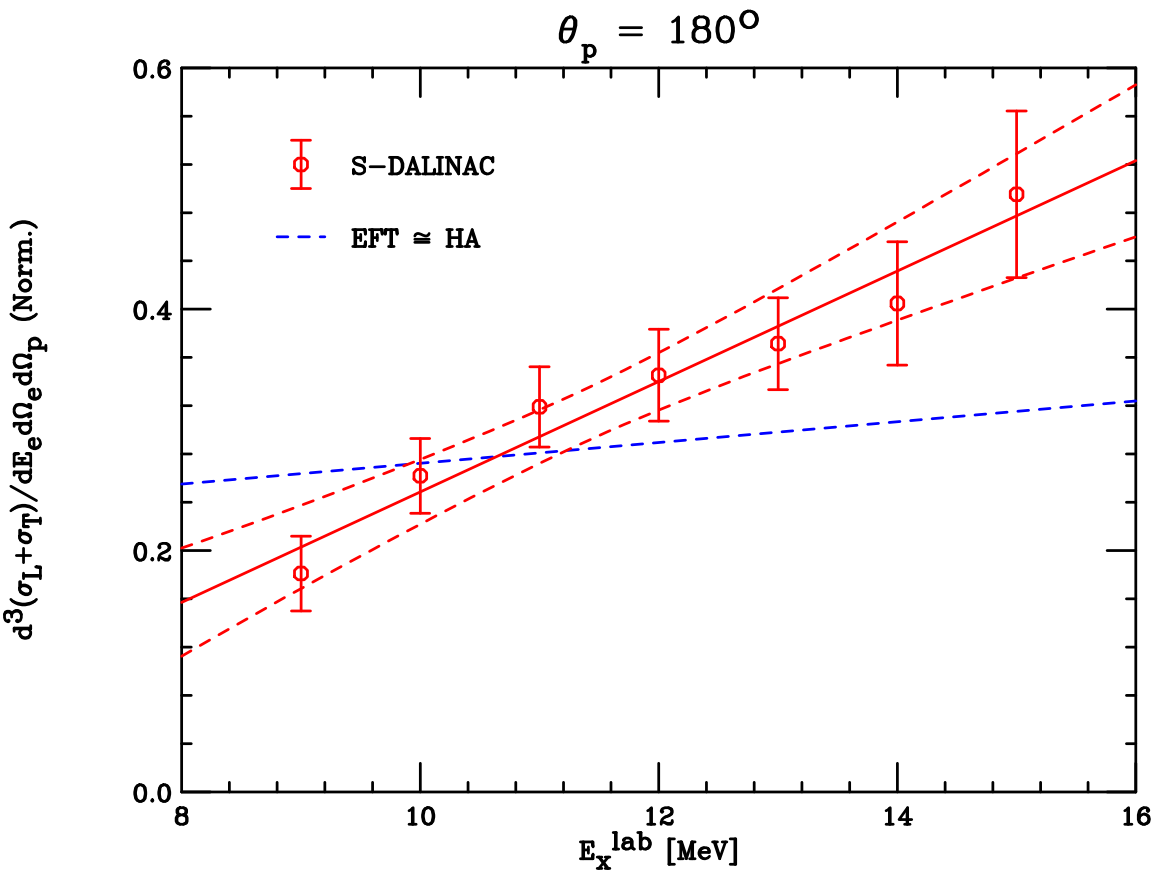

Figure 2: Measurement of the combined longitudinal and transverse cross sections within a small acceptance centred on 180^o from von Neumann $et\ al.$ [11]. The solid red line is a linear fit to the data and the red dashed lines represent the 68% confidence interval of the fit. The blue dashed line is the EFT calculation of Christlmeier and Griesshammer [12] which is essentially indistinguishable from that of Schmitt and Arenhoevel [10].

Source (LEGS) at Brookhaven [14] support the conclusions drawn from the previous three data sets that something not understood is taking place when the outgoing pn system has an internal energy of about $9\ MeV$. Figure 3 shows the two data sets. The upper panel shows the MMF measurements of the missing mass of the outgoing pn system from the reaction $d\,(p,pp)\,X$. The center (lower) panel shows the LEGS measurements of the missing mass of the outgoing nn system (X) from the reaction $\vec{\gamma} + d \rightarrow X + \pi^+;\ X \rightarrow n + [n] + [\gamma']$ when the π^+ was emitted parallel (perpendicular) to the plane of the incident photon polarization. The particles in square brackets were detected to identify the specific reaction but were not used in the calculation of missing masses. The agreement between the peak positions is striking although perfect agreement would not be expected as in MMF case the outgoing system was composed of a pn pair while in the LEGS case the outgoing system was composed of an nn pair. Here again, the missing mass of the lowest observed structure in the LEGS data corresponds to an nn system with an internal energy of about $9\ MeV$. It is to be noted that the clear discrepancies seen in both the Nath and Cichocki data involved polarization observables. For this reason we are anxious to pursue studies of polarization observables in this reaction.

The lower energy region of photodisintegration gives unique conditions for constraining models. The uncertainties concerning relativistic corrections and isobar configurations are greatly suppressed in addition to strongly satisfying gauge independence of nonrelativistic calculations.

No photodisintegration tensor polarized asymmetry data have been taken for photon energies below 40 MeV. However, there have been measurements at higher energy performed at the 2 GeV electron storage ring VEPP-3 [15]. Fig. 4 shows the data from this experiment. In this experiment a thin-wall open-ended storage cell fed by polarized deuterium gas from an Atomic Beam Source (ABS) was used as an internal target. The ABS provided a polarized deuterium gas jet with an intensity of up to 8×10^{16} atoms/s with tensor polarization above P_{zz} $\sim$98%, while the vector polarization was close to zero ($|P_z| < 0.02$).

The goal of the measurements proposed here is to obtain high precision data on T_{20} for the photon energy range of $4\ MeV \ \leq \ E_\gamma \ \leq \ 20\ MeV$ over a fine grid of neutron emission angle. These data will place stringent constraints on current models of the deuteron as well as shed light on the previously observed discrepancies. The potential impact of these measurements is hard to overstate. If the current models are confirmed then it will bring into serious question the previous contradicting results. Were they simply wrong? Or are the origins of the effects seen even more subtle? If the previous anomalous measurements are confirmed, then a plethora of questions about the two-nucleon system will open:

- do narrow, relatively long-lived NN states exist?
- what would this tell us about the NN interaction?
- what is the structure/configuration of such states?
- what role could such states play in our understanding of other phenomena such as neutron stars?
- what role would a reaction channel producing such states play in modifying detailed balance shortly after the Big Bang?

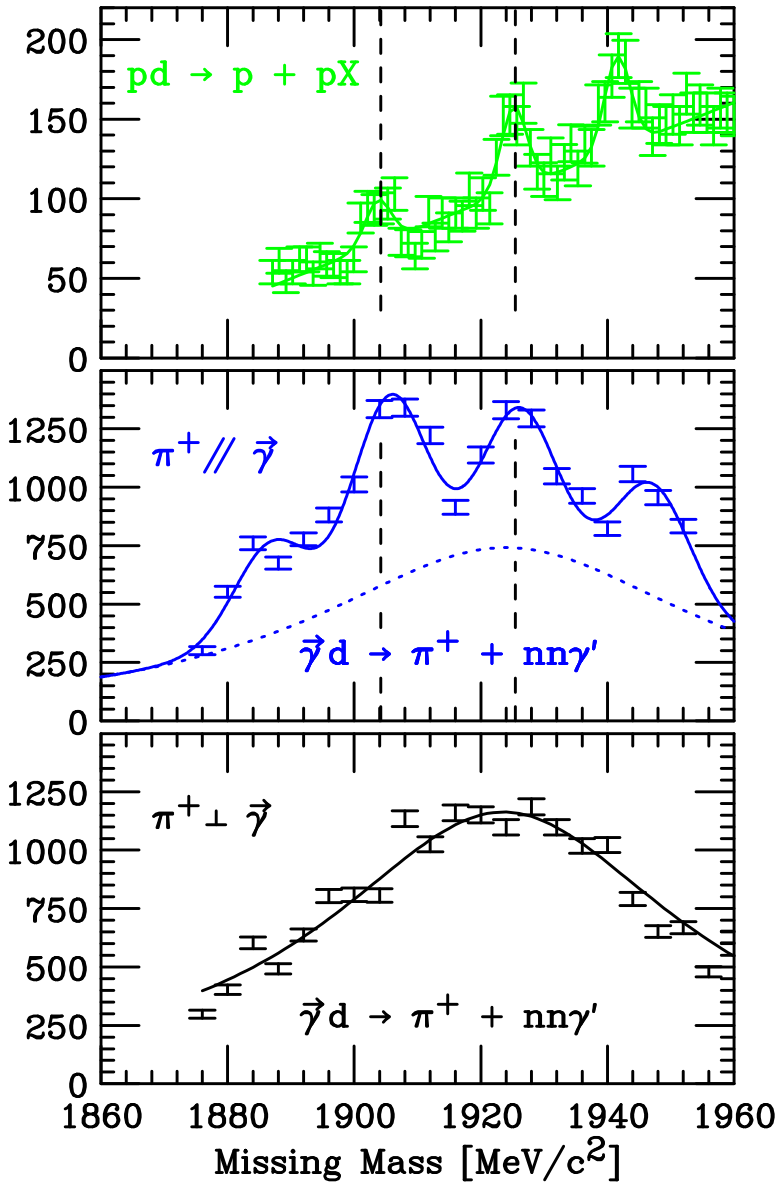

Figure 3: The top panel shows the data of Fil'kov $et\ al.$[13] for the reaction $d(p,pp)X$; the middle (bottom) panel shows the data of Cichocki $et\ al.$ for the reaction $d\,(\vec{\gamma},\pi^+[n\gamma'])\,X$ in which the π^+ is emitted parallel (perpendicular) to the polarization plane of the incident photon. Particles in the square brackets were detected to identify the reaction but were not used in computing the missing mass of the intermediate state.

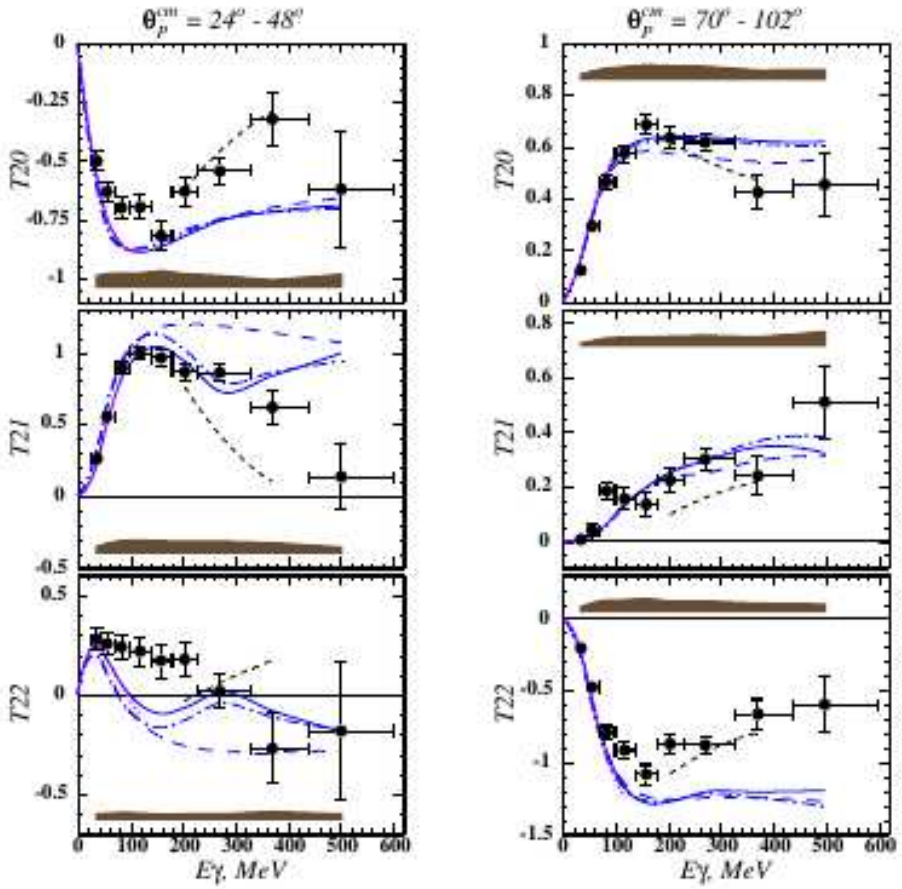

Figure 4: The tensor analyzing powers with respect to photon energy for VEPP-3 experiment [15] with theoretical predictions from [10] "N+MEC" (blue long-dashed line), "N+MEC+IC+RC" (solid line) models, from [16] (magenta dotted line), and from [17] (black short-dashed line). Figure from [15].

- what role would such a channel play in the early stages of nucleosynthesis?
- how would such states contribute to our understanding of short-range correlations in nuclei?

Either way, the results promise to be exciting.

2.2 Other HI$\vec{\gamma}$S Activity

The collaboration submitting the present proposal consists of a set of collaborators who have been working toghether at HI$\vec{\gamma}$S for some time: B. Norum, D. Crabb $et\ al.$ of the University of Virginia, R. Pywell $et\ al.$ of the University of Saskatchewan, and B. Sawatzky of Jefferson Lab. Joining in this proposal, and new to working at HI$\vec{\gamma}$S, are D. Day, D. Keller $et\ al.$ also from the University of Virginia, as well as D. Higinbotham of Jefferson Lab. Theorists H. Arenhoevel (Mainz) and S. Liuti (UVA) have also joined to provide assistance in interpretation and evaluation of the results. Two of the spokespersons, P. Seo and B. Norum, have been heavily involved in work at HI$\vec{\gamma}$S for some time.

The proposed experiment is closely related to two experiments currently in preparation for running at HI$\vec{\gamma}$S. The first is the measurement of the Gerasimov-Drell-Hearn Sum Rule for the deuteron. After the serious setback that resulted from the unexplained accidental damage to the HIFROST target, we are currently on course to run this experiment later this year. We are also preparing to measure the reaction $d\left(\vec{\gamma},\vec{n}\right)p$. The first of ten neutron polarization analyzer cells has been filled and successfully tested with a radioactive source. The principal goal of this experiment is to confirm or refute the results of Nath $et\ al.$ but will extend to double polarization measurements as well.

The initial UVA-USask-JLAB collaboration is also preparing two additional experiments not directly related to the current proposal. These involve 1) measurements of ${}^4He\left(\vec{\gamma},n\right){}^3He$ and ${}^4He\left(\vec{\gamma},n\right)dp$ and 2) measurements of asymmetries in the Bethe-Heitler process.

2.3 Collaboration Responsibilities

While there is necessarily much overlap among the activities of the various collaborators, the breakdown of the work will be roughly as follows. The UVA group will have principal responsibility for the polarized target as well as overall coordination. The UVA, USask, and JLAB groups will have joint responsibility for the Blowfish detector with the USask and JLAB groups focusing on the electronics and DAQ. The USASK group is also leading the Monte Carlo effort. Theorists at UVA and Mainz will focus on the analysis and interpretation of results. The excellent and invaluable engineering and technical contributions of the TUNL/HI$\vec{\gamma}$S staff must also be recognized.

It is anticipated that one or two students will derive PhD dissertations from this work. One will definitely be able to obtain a dissertation from the T_{20} measurement; another may be able to obtain a more technically oriented dissertation from the target development.

3 Experiment Description

The proposed experiment will utilize the dilution refrigerator of the HI$\vec{\gamma}$S Frozen Spin Target (HIFROST) with a longitudinally polarized holding field and an additional microwave coil, the Blowfish neutron detector array, and the Saskatchewan five-paddle beam monitor calibrated against a NaI detector. The LUCID-ROOT data acquisition system developed at the University of Saskatchewan will be used.

3.1 Tensor Polarization

Following the notation of Schmitt and Arenhoevel[10], the cross-section of the two-body PD of the polarized deuteron (unpolarized photon) can be expressed as,

$$\begin{aligned}\frac{d\sigma}{d\Omega} &= \frac{d\sigma_0}{d\Omega}\{1 - \sqrt{3/4}P_z \sin\theta_{d\gamma} \sin\phi T_{11}\left(\theta_p^{cm}\right) \\ &+ \sqrt{1/2}P_{zz}[(3/2\cos^2\theta_{d\gamma} - 1/2)T_{20}\left(\theta_p^{cm}\right) \\ &- (\sqrt{3/8}\sin 2\theta_{d\gamma}\cos\phi T_{21}\left(\theta_p^{cm}\right) \\ &+ (\sqrt{3/8}\sin^2\theta_{d\gamma}\cos 2\phi T_{22}\left(\theta_p^{cm}\right)]\}\end{aligned} \quad (1)$$

where σ_0 is the unpolarized cross-section, P_z (P_{zz}) is the degree of vector (tensor) polarization, $\theta_{d\gamma}$ is the angle between the polarization axis and the momentum of the γ-quantum, and ϕ is the angle between the polarization plane and the reaction plane. The tensor analyzing powers T_{2I} are functions of photon energy E_γ and proton emission angle θ_p^{cm}.

The most basic theoretical prediction starts with a calculation [10] using a one-body current using the Bonn OBEPR NN potential with the major part of meson exchange currents (MEC), this model is denoted as "normal" (N). Adding the pion exchange currents ("+MEC"), isobar configurations ("+IC") and the leading order relativistic corrections ("+RC") are added. The calculation of [16] includes heavy-meson and all MEC diagrams with isobar configurations and relativistic corrections added. The calculation pertains to E_γ below the pion production threshold. The deuteron PD above pion production threshold is investigated in [17] in a coupled-channel approach with $N\Delta$ and πd channel, using a dynamic treatment of the pions. As a result the NN potential and $\pi - MEC$ become retarded and electromagnetic loop corrections are included.

When a spin 1 system such as the deuteron is subjected to a magnetic field along the z-axis, the Zeeman interaction gives rise to three magnetic sublevels $I_z = +1, 0, -1$ with population fractions p_+, p_-, p_0, respectively. These populations are described by both a vector polarization,

$$\begin{aligned}P_z &= \langle I_z/I\rangle \\ &= (p_+ - p_0) + (p_0 - p_+) = p_+ - p_-\end{aligned} \quad (2)$$

and a tensor polarization [18]:

$$\begin{aligned}P_{zz} &= \langle 3I_z^2 - I(I+1)\rangle/I^2 \\ &= (p_+ - p_0) - (p_0 - p_-) = 1 - 3p_0\end{aligned} \quad (3)$$

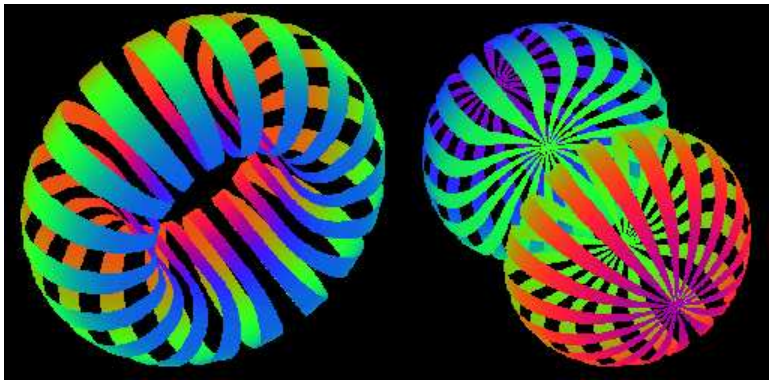

Figure 5: Nucleon densities of the deuteron in its two spin projections, $I_z = 0$ and $I_z = \pm 1$, respectively. *Reproduced from [19, 20]*.

which are subject to the overall normalization $p_+ + p_- + p_0 = 1$.

Fig. 5 graphically demonstrates the dependence of the two nucleon distribution on the spin projection. If the two nucleons are in a relative $m = 0$ state, the surface of constant density is toroidal, while if they are in the $m = \pm 1$ state, the surface has a dumbbell shape.

In the case of deuteron spins in thermal equilibrium with the solid lattice, and neglecting the small quadrupole interaction [18], the tensor polarization is related to the vector polarization via:

$$P_{zz} = 2 - \sqrt{4 - 3P_z^2} \tag{4}$$

The maximum absolute value of $P_{zz} = -2$ occurs only for vanishing populations in the $m = \pm 1$ states. If, on the other hand, only the $m = 1$ or $m = -1$ state are occupied, the vector polarization reaches its maximum value of $+1$, and $P_{zz} = +1$.

It is the requirement that one have a very high degree of vector polarization in order to obtain a possibly useful degree of tensor polarization that has inhibited the use of thermally equilibrated targets. The upcoming measurements at HI$\vec{\gamma}$S of the GDH Sum Rule on the deuteron will be sensitive to the tensor polarization of the target and will have to take some data using a depolarized target in order to correct for it. Unfortunately, the precision of those measurements will be inadequate to address the physics issues on which the current proposal is focused.

The experimental tensor target asymmetry can be achieved using three different helicity configurations. This is expressed as

$$a_T = \sqrt{2}\left(\frac{N^+ - N^-}{P_{zz}^+ N^- - P_{zz}^- N^+}\right) = \sqrt{2}\left(\frac{N^+ - N}{P_{zz}^+ N}\right) = \sqrt{2}\left(\frac{N^- - N}{P_{zz}^- N}\right) \tag{5}$$

where $N^+(N^-)$ is the number of events detected with positive (negative) target polarization and N is the number of events detected with a unpolarized target. The tensor asymmetry can be found using positive and negative tensor polarization, or just positive tensor polarization and an unpolarized target, or just negative tensor polarization and an unpolarized target. With the goal of mitigating the vector polarization it is most convenient to use a negatively tensor polarized target and an unpolarized target.

It is possible to isolate the three components of tensor analyzing power by collected data using three different polarization axes, specified by $\theta^n_{\gamma d}$ with respect to the beam-line: The angles $\theta^0_{\gamma d} = 0^\circ$, $\theta^1_{\gamma d} = 54.7^\circ$ and $\theta^2_{\gamma d} = 125.3^\circ$, with ϕ close to 0°. The target asymmetry is then proportional to $a^T_0 \sim c_0 T_{20}$, $a^T_1 \sim -c_1 T_{21} + c_2 T_{22}$ and $a^T_2 \sim c_1 T_{21} + c_2 T_{22}$ where c_i are constants defined by the geometry of detector and target configuration. The term with T_{11} can be suppressed in two different ways, first through the $\sin\phi$ dependence and second by mitigating the vector polarization P_z.

Polarizing deuterium with T_{21} and/or T_{22} components in a frozen spin solid target will require the installation of addition magnetic coils surrounding the target cell. Fortunately, one of the two developments we undertook to recover from the unexplained damage to the target that occured over a year ago entailed expanding the target containment vessel. It appears likely that this will give us enough room to accommodate the additonal coils. Doing so will be the object of subsequent work if the results from the proposed measurements indicate that it might be fruitful.

3.2 Polarized Target

This experiment will use the HIFROST target fridge, see Fig. 6. The target is typically polarized at a higher temperature ∼1K, and set in frozen spin mode by running at lower temperature ∼30-50 mK. The cooldown of the magnet from room temperature to 4 K takes about 6 hours. The dilution refrigerator is then cooled in 2 hours to 1 K, the cells of the target holder are filled with the material and the target holder is pushed into the precooled mixing chamber. Purging, final cooldown and condensing the ^{4}He-^{3}He mixture takes less than 1 hours. During DNP the temperature of the helium mixture decreases slowly from about 350 mK to 200 mK as the optimum microwave power is reduced with increasing polarization. The expected DNP vector polarization is greater than 80%. This can be greater negative polarization. polarization is reached in 12 hours of DNP. The target is cooled down below 100 mK by turning the microwave power off 0.5-1 hours before the field rotation. The ultimate temperature is reached only after several hours of running without microwaves. After circulating the ^{3}He for several minutes and fridge will begin to dilute and the temperature gradually drops to about 30 mK.

Figure 7 shows the NMR signal and polarization growth curve of deuterated propanediol doped with OXO63. Irradiated d-butanol is expected to perform on a similar level.

3.2.1 Enhanced Tensor Polarization

Deuteron spin alignment can be manipulated when exposed to a modulated RF field using an external coil around the target cup, as seen if Figure 12. The accuracy and enhancement of the tensor polarization is greatly dependent on the polarization technique. Tensor polarization can be measured when the magnetic sublevels are out of the Boltzmann distribution when the intensities I_+ and I_- of each peaks in the NMR signal represent the total area of each independent transition probability distribution, see Figure 11. The tensor polarization under any spin distribution can be described as,

$$P_{zz} = C(I_+ - I_-). \tag{6}$$

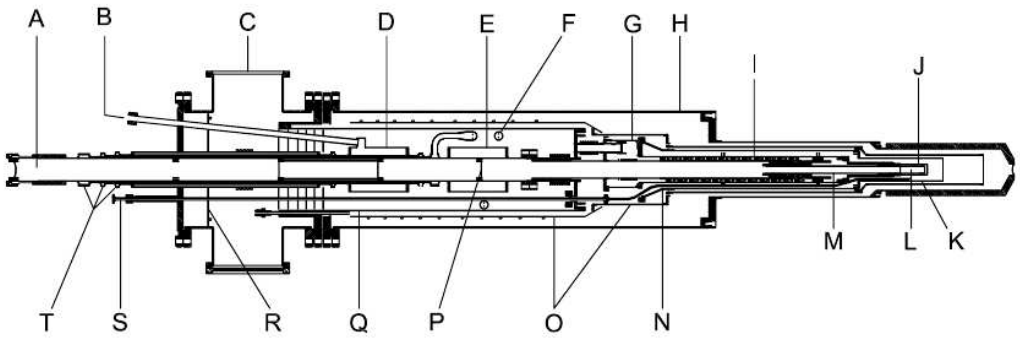

Figure 6: Cross section view of the HIFROST target fridge. A: beam pipe, B: LHe inlet, C: 3 He pump port, D: 4 K pot, E: 1 K pot, F: 1 K heat exchanger, G: still, H: vacuum chamber, I: sintered heat exchanger, J: mixing chamber, K: holding coil, L: target cup, M: target insert, N: 1 K heat shield, O: 20 K heat shield, P: beam pipe heat shield (one of three), Q: 3 He pump tube, R: copper cold plate, S: waveguide, T: precool heat exchanger. The overall length of the cryostat is approximately 2 m.

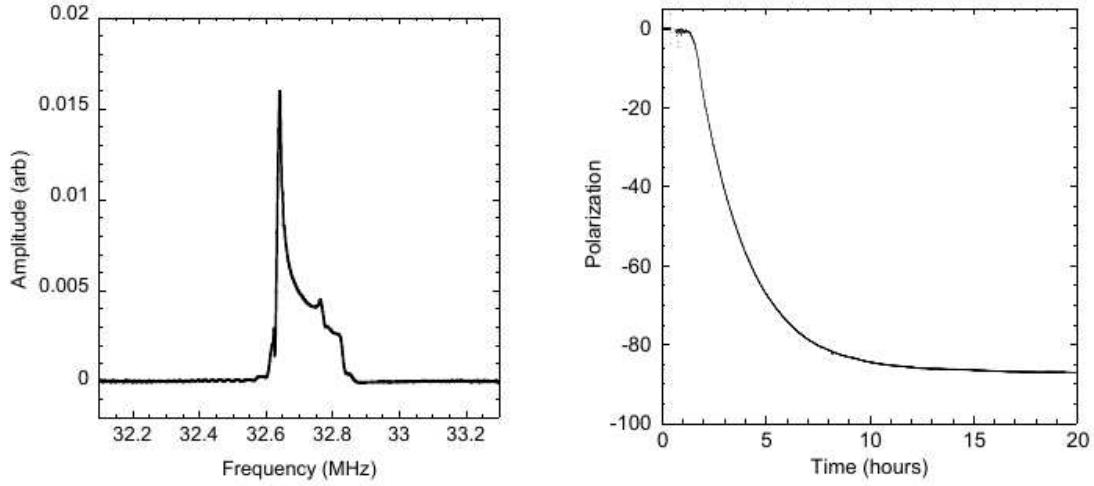

Figure 7: Performance of the signal and polarization growth curve of deuterated propanediol doped with OXO63 from Jlab Hall-B Frost experiment.

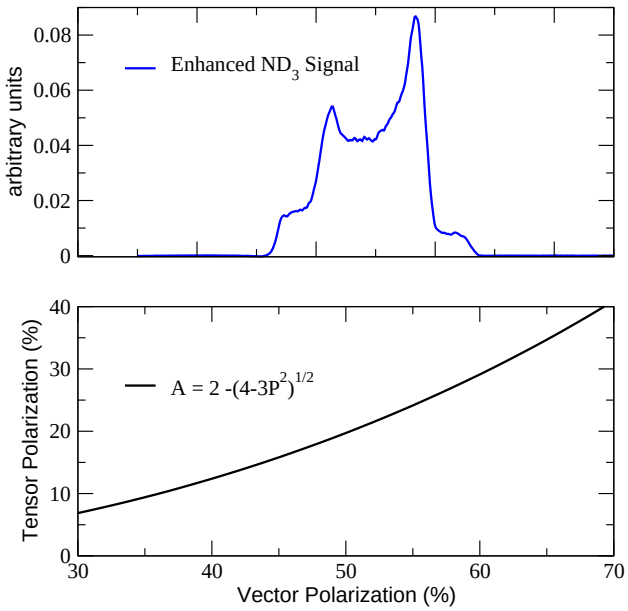

Figure 8: **Top**: NMR signal for ND_3 with a vector polarization of approximately 50% from the GEN experiment. **Bottom**: Relationship between vector and tensor polarization in equilibrium, and neglecting the small quadrupole interaction.

Here C is the calibration constant. A positive tensor polarization enhancement occurs only when the $n_+ + n_-$ population increases with respect to n_0 population. To optimize positive tensor polarization the vector polarization must be maximized using DNP at which point the microwave is turned off and the RF-modulation begins. The RF-modulation induces transition at the frequency domain that is spans. Tensor polarization optimization will occur when the range in RF-modulation is chosen as to maximize the difference in the intensities I_+ and I_- throughout the signal.

Negative tensor enhancement can be achieve by proton deuteron cross-polarization which fills the $m = 0$ sublevel directly from the spin reservoir of another (proton) system [21]. The deuteron spin system is polarized using strong thermal contact between the proton spin-spin interaction reservoir and the deuteron quadrupole interaction reservoir. The thermal contact is maintained using high powered RF just off of the Larmor frequency of the two spin species. As the $m = 0$ sublevel is filled there are transition of equal likelihood to the greater or less energy levels so the NMR signal using this type of cross polarization has both absorption and emission. The greater the proton spin-spin reservoir the greater the tensor polarization achievable in the deuteron. This can be done to achieve a near zero vector polarization however the maximum tensor polarization that can be acquired for the thermal conditions of the Duke/UVA cryostat has yet to be studied. Measuring and fitting techniques for RF manipulated deuteron NMR lines have been recently developed at UVA. The theoretical lineshape for d-butanol polarized using proton deuteron cross-polarization is show in Fig. 9.

A selective AFP (Adiabatic Fast Passage) can also be used to achieve negative tensor polarization. An AFP [22, 23] is a reverse in the polarization using a single RF sweep which is slow enough to follow the Adiabatic Theorem but is still fast with respect to the relaxation rates of the material

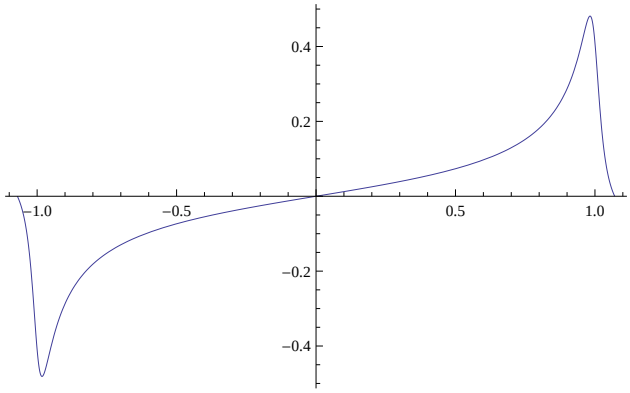

Figure 9: The theoretical lineshape for d-butanol polarized using proton deuteron cross-polarization .

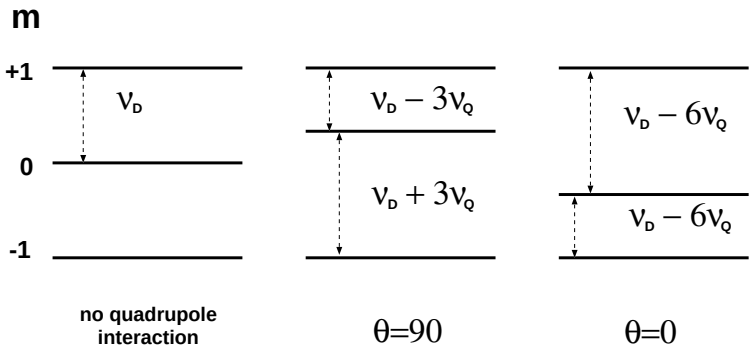

Figure 10: Energy levels in d-butanol. The level spacing is shifted by the quadrupole interaction, which depends on the angle θ between the magnetic field and the electric field gradient.

at the temperature and field conditions. The spins effectively follow the magnetic field of the RF sweep as it passes through the resonance line resulting in a helicity flip of the target. A selective AFP is when the RF is swept through a specific frequency domain to selectively manipulate the deuteron alignment. UVA has recently achieved this with d-butanol at 5 T and 1 K.

Negative tensor polarization is especially interesting because not only is it easier to hold zero vector polarization but the magnetic sublevels $m = +1$ and $m = -1$ are depleted to both fill the $m = 0$ sublevel leading to a magnetization reservoir that is twice as large. This doubling of the polarization reservoir is only useful when the target state can be held long enough to take data in an experiment. This is easily achieved when using a Frozen Spin Target where the temperature of the material is held below 100 mK slowing the relaxation rates, effectively Freezing the polarization in place.

3.2.2 Polarization Analysis

The three Zeeman sublevels of the deuteron system ($m = -1, 0, 1$) are shifted unevenly due to the quadrupole interaction [18]. This shift depends on the angle between the magnetic field and

the electrical field gradient, and gives rise to two separate transition energies. Hence, the unique double peaked response displayed in Fig. 8.

The energies [24] of these three magnetic sublevels are:

$$E = -h\nu_D m + h\nu_Q \left[(3\cos^2(\theta) - 1\right] \left[3m^2 - I(I+1)\right] \tag{7}$$

where ν_D is the deuteron Larmor frequency and ν_Q is a function of the deuteron quadrupole moment eQ. The quadrupole interaction shifts these levels depending on the angle θ between the magnetic field and the electrical field gradient, as shown in Fig. 10.

When the system is at thermal equilibrium with the solid lattice, the deuteron polarization is known from:

$$P_z = \frac{4 + \tanh \frac{\mu B}{2kT}}{3 + \tanh^2 \frac{\mu B}{2kT}} \tag{8}$$

where μ is the magnetic moment, and k is Boltzmann's constant. The vector polarization can be determined by comparing the enhanced signal with that of the Thermal Equilibrium (TE) signal (which has known polarization).

Measurements of the deuteron polarizations using CW-NMR contain more information for the polycrystalline materials such as deuterated butanol and deuterated ammonia. The two overlapping absorption lines are analyzed to determine the signal intensities I_+, I_- resulting in an approximated relative population of the magnetic sublevels. When these sublevels exist under a Boltzmann distribution obtaining polarizations are particularly simple and with well managed errors. The target spin orientation can be described using the vector and tensor polarization. Tensor polarization can be expressed in terms of the vector polarization as $P_{zz} \doteq 2 - \sqrt{4 - 3P^2}$ where the dot implies the relation is true when thermal equilibrium exists within the deuteron spin species. The definition of vector polarization for spin-1 is,

$$P = \frac{n_+ - n_-}{n_+ + n_- + n_0} \doteq \frac{r^2 - 1}{r^2 + r + 1}, \tag{9}$$

with the tensor polarization defined as,

$$P_{zz} = \frac{n_+ - 2n_0 + n_-}{n_+ + n_- + n_0} \doteq \frac{r^2 - 2r + 1}{r^2 + r + 1}. \tag{10}$$

Where the second equality in each case is not part of the definition but a relation to the transition ratio r defined as $r = I_+/I_-$, see Figure 11. These relations in terms of $r = e^{\beta\hbar\omega_d}$ are true to first order in $\beta\hbar\omega_q$, where ω_d (ω_q) is Larmor (quadrupole interaction) frequency. The intensities I_- and I_+ can be determined using a fitting procedure resulting in the value of the transition ratio. The resulting polarization measurements can be used complementary to the TE signal polarization calibration. Both vector and tensor polarization can be determine this way to errors less that 3%. The TE used in acquisition of the calibration constant and the analysis of the lineshape are required once the distribution of spin states in the target have been disturbed and no longer follow a Boltzmann distribution.

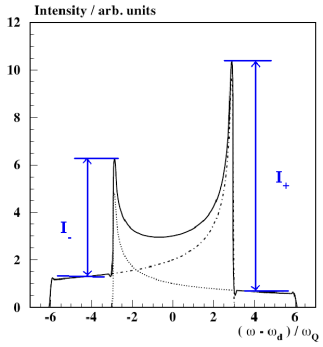

Figure 11: Deuteron Magnetic Resonance line shape and peak intensities I_+ and I_-.

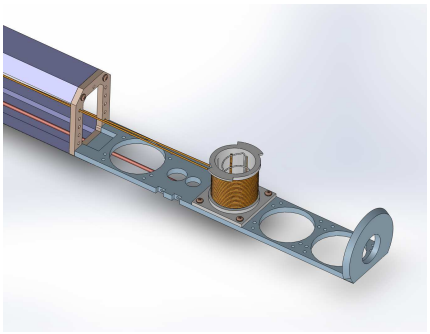

Figure 12: Diagram Target test cup and coil used to generate the modulated RF field.

3.2.3 Depolarizing the Target

To move from polarized to unpolarized measurements, the target polarization will be annihilated using destructive RF modulation while leaving the cryostat in the exact same state. This ensure that there are no changes from one helicity state to the other that can result in false asymmetry contributions. NMR measurements will be used to confirm destruction of the polarization. The target material will be held at a constant temperature, and the target field will be held at a constant magnitude for both polarized and unpolarized data collection. in order to minimize the systematic differences in the two states.

3.3 Experimental Method

The measured PD cross section for a spin-1 target characterized by a vector polarization P_z and tensor polarization P_{zz} from Eq. 2 can be simplified for $\theta = 0^\circ$ such that,

$$\frac{d\sigma_p}{d\Omega} = \frac{d\sigma_0}{d\Omega}\left(1 - P_z\Sigma + \frac{1}{\sqrt{2}}P_{zz}a^T\right), \tag{11}$$

where, σ_p (σ) is the polarized (unpolarized) cross section, Σ (a^T) is the vector (tensor) asymmetry of the PD deuteron cross section. This allows us to write the positive polarized, $0 < P_{zz} \leq 1$, or the negative polarized, $-2 < P_{zz} \leq 0$, tensor asymmetry using unpolarized photon beam as,

$$a^T = \frac{2}{P_{zz}}\left(\frac{\sigma_1}{\sigma} - 1\right)A \tag{12}$$

where σ_1 is the polarized cross section for

$$P_{zz} = \frac{n_+ - 2n_0 + n_-}{n_+ + n_- + n_0}. \tag{13}$$

Here n_m represents the portion of the ensemble in the m state.

Eq. 12 reveals that the asymmetry a^T compares two different cross sections measured under different polarization conditions of the target, positively tensor polarized and unpolarized. To obtain the relative cross section measurement in the same configuration, the same target cup and material will be used at alternating polarization states (polarized vs. unpolarized), and the magnetic field providing the quantization axis will be oriented along the beamline at all times. This field will always be held at the same value, regardless of the target material polarization state.

Since many of the factors involved in the cross sections cancel in the ratio, Eq. 12 can be expressed in terms of the yield normalized, efficiency corrected numbers of tensor polarized N_1^c and unpolarized N^c counts,

$$a^T = \frac{2}{P_{zz}} \left(\frac{N_1^c}{N^c} - 1 \right) \tag{14}$$

The time necessary to achieve the desired precision δa^T is:

$$T = \frac{N_T}{R_T} = \frac{4}{P_{zz}^2 \delta (a^T)^2 R_T} \tag{15}$$

where R_T is the total rate and $N_T = N^1 + N$ is the total estimated number of counts to achieve the uncertainty δa^T.

3.3.1 Statistical Uncertainty

To investigate the statistical uncertainty we start with the equation for a^T using measured counts for polarized data N_1 and unpolarized data N,

$$a^T = \frac{\sqrt{2}}{P_{zz}} \left(\frac{N_1}{N} - 1 \right). \tag{16}$$

The absolute error with respect to counts in then,

$$\delta a^T = \frac{\sqrt{2}}{P_{zz}} \sqrt{\left(\frac{\delta N_1}{N} \right)^2 + \left(\frac{N_1 \delta N}{N^2} \right)^2}. \tag{17}$$

For small asymmetries, $N_1 \approx N$, so that twice N is required to obtain the total number of counts N_T for the experiment. This leads to:

$$\delta a^T = \frac{2}{P_{zz}} \frac{1}{\sqrt{N_T}}. \tag{18}$$

Under the assumed running conditions this means that our statistical precision in each detector will average

$$\delta a^T \approx 0.003. \tag{19}$$

but will range up to 0.01 near $\theta_n = 90^o$ where the cross section is quite insenstive to T_{20} anyway.

Source	Systematic
Polarimetry	6.0%
Packing fraction	2.0%
Detector Drift	1.0%
Photon Flux (absolute)	2.0%
Photon Flux (stability)	1.0%
Reconstruction resolution and efficiency	1.0%
Total	6.8%

Table 1: Estimates of the scale dependent contributions to the systematic error of a^T.

3.3.2 Systematic Uncertainties

Table 1 shows a list of the scale-dependent uncertainties contributing to the systematic error in a^T. The uncertainty associated with measuring the target polarization is discussed in Sect. 3.2.2. The uncertainty associated with the packing fraction reflects the uncertainty in real target (deuteron) thickness sampled by the photon beam. It arises from possible variation in the photon beam intensity profile across the target cell. The time variation in detector response is monitored continuously by pulsing each of the 88 Blowfish cells with light via optical cables from a central source. The stability of the source is sufficient to ensure that the Blowfish detector responses are stable within this range. The five-paddle beam monitor has been shown to achieve this resolution by comparison to a highly efficient NaI detector.

Eq. 14 involves the ratio of counts, which leads to cancellation of several first order systematic effects. However, the fact that the two data sets will not be taken simultaneously leads to a sensitivity to time dependent variations which will need to be carefully monitored and suppressed. To investigate the systematic differences in the time dependent components of the integrated counts, we need to consider the effects from calibration, efficiency, acceptance, and luminosity between the two polarization states.

In order to look at the effect on a^T due to drifts that affect the luminosity measurement over time such as calibration and detector efficiency, we rewrite Eq. 14 explicitly in terms of the raw measured counts N_1 and N,

$$\begin{aligned} a^T &= \frac{2}{P_{zz}}\left(\frac{N_1^c}{N^c}-1\right) \\ &= \frac{2}{P_{zz}}\left(\frac{Q\varepsilon l\mathcal{A}}{Q_1\varepsilon_1 l\mathcal{A}}\frac{N^1}{N}-1\right) \end{aligned} \tag{20}$$

where Q represents the accumulated photon flux, and ε is the detector efficiency. The target length l and acceptance $\mathcal{A}$ are identical in both states, to first order.

We can then express Q_1 as the change in photon intensity calibration that occurs in the time it takes to collect data in one polarization state before switching such that $Q_1 = Q(1-\delta Q)$. In this notation, δQ is a dimensionless ratio of photon flux in the different polarization states. A similar

representation is used for drifts in detector efficiency leading to,

$$a^T = \frac{2}{P_{zz}} \left(\frac{N_1 Q(1-\delta Q)\varepsilon(1-\delta\varepsilon)}{NQ\varepsilon} - 1 \right). \tag{21}$$

which leads to,

$$a^T = \frac{2}{P_{zz}} \left(\frac{N_1}{N}(1 - \delta Q - \delta\varepsilon + \delta Q\delta\varepsilon) - 1 \right). \tag{22}$$

We can obtain estimates of δQ and $\delta\varepsilon$ from previous experiments as the Five Paddle Monitor has been used extensively. We can also draw on the experience of the similar FROST target at Jefferson LAB. For the present proposal, we use the same estimate except that the period between target polarization states is ≈ 6 hours rather than 3 months, leading to an overall drift $\delta\epsilon \sim 0.01\%$. To express a^T in terms of the estimated experimental drifts in efficiency and photon flux measurement we can write,

$$a^T = \frac{2}{P_{zz}} \left(\frac{N_1}{N} - 1 \right) \pm \frac{2}{P_{zz}} \delta\xi. \tag{23}$$

where $\delta\xi = \delta Q + \delta\varepsilon$. This leads to a contribution to a^T on the order of 1×10^{-3},

$$da^T_{drift} = \pm \frac{2}{P_{zz}} \delta\xi = \pm 4 \times 10^{-3}. \tag{24}$$

which is comparable to the average statistical precision for individual detectors.

The polarization state of the target will be changed about every 6 hours, so at each of our settings we expect only one polarization cycle pair. If there are false asymmetries that arise on this time scale it is possible to use an adiabatic fast passage (AFP) to change quickly between positive and negative polarization rather than using unpolarized. This could greatly increase the number of helicity flips per kinematic setting. The efficiency of this procedure has not been studied for this purpose and is not planned to be used unless required, we are fully comfortable with our operational understanding of it, and we are confident that the introduction of a second target polarization measurement will not introduce more uncertainty.

The identical configuration of the two polarization states minimizes the relative changes in luminosity with respect to time. Fluctuations in luminosity due to target density variation can be kept to a minimum by keeping the material beads at the same temperature for both polarization states through control of the microwave and the LHe evaporation. The He vapor pressure reading provides an accuracy of material temperature changes at the level of $\sim$0.1%.

The reconstruction resolution and efficiency includes the effects of the GEANT Monte Carlo simulations of the detector response. This was tested in July 2015 in a run with 9 MeV circularly polarized gammas. Three detectors were all placed at a scattering angle of 90^o but each under different conditions. Two were placed adjacent to each other with one surrounded on four sides by neutron shielding. The other was placed adjacent to the first with no shielding save for that provided by the first detector. The third detector was placed on the opposite side of the beam line near an aluminum structure of sufficient mass to be a source of scattered neutrons. The observed rates in the three detectors differed by up to 15%. After corrections were applied based on a

GEANT simulation assuming $d(\gamma, n)p$ cross sections based on the calculations of Schmitt and Arenhovel [10] all three agreed to with $\pm$0.5%.

The projected counting rate will yield an average statistical precision of approximately 0.25% per detector per run, albeit rather unevenly distributed among the 88 detectors as count rates in individual detectors will vary by factors of up to 10. The anticipated statistical precision is significantly better than the anticipated systematic precision which is dominated by the measurement of the target polarization (6%). However, in extracting the asymmetry we are comparing a measurement using a target with a finite tensor polarization and one using a target with no polarization. The absence of polarization can be established to very high precision so the target polarization uncertainty affects only one measurement and does so in the form of a scaling factor affecting all terms in the expansion of the analyzing power equally. Thus, it will not affect our ability to extract to high precision the relative magnitudes of the terms in the analyzing power.

4 Run Plan

The schedule will be dictated primarily by the running of the GDH measurement. The target cell required for the tensor polarized target will be developed in parallel but no alterations to the HIFROST will be made until the completion of the GDH experiment. We expect to run the GDH experiment this summer (2016) so modifications are expected to begin this fall. The earliest we could expect to be able to run this experiment is during the first half of 2017.

For all planned beam energies, there are no completing sources of neutrons with energies close to those from deuteron photodisintegration. Thus, we can estimate our efficiency for extracting real events based on past experience with D_2O targets. We have planned the running based on

- the assumption that the accelerator will be operational for two eight-hour shifts per day,
- that the fluxes shown on the TUNL/HIGS website will be available, and
- that the rate at which we can accumulate final data (after ADC, TOF, PSD, etc. cuts) is 1 kHz. With first half of the time spent using the target polarized and the second half with the target depolarized we will gather approximately 4×10^7 events per day, roughly half for each target state.

The night shift will be used for repolarizing the target, transferring liquid helium between dewars, annealing the target material when necessary, and any other operations that do not require the beam.

The decision to request running with one energy per day rather than attempt to more finely tune the beam times for each energy was based on an evaluation of the overall efficiency of the experiment. Changing the beam energy during the active accelerator shifts would entail using possible data acquisition time to retune the accelerator and to repolarize (and measure) the target. Tuning the accelerator once per day was felt to be optimal.

We would prefer to run the experiment in a single period. Once the target and other systems have been made operational we feel it would be most efficient to run continuously.

Setup for the experiment will take approximately two weeks once the Gamma Vault has been cleared. It will require

- configuring, cooling, testing the HIFROST (including the gas handling, microwave, NMR, and monitoring systems).
- setting up the 88 cells of the Blowfish. This could take somewhat longer if the $d\,(\vec{\gamma}, \vec{n})$ experiments runs before the experiment proposed here as that experiment will entail removing and reconfiguring approximately 64 cells from the Blowfish.
- setting up, testing, and calibrating the Five-Paddle beam monitor.
- setting up the data acquisition electronics and LUCID software.

Decommissioning the experiment will take approximately one week.

Both the cross section and the tensor analyzing power vary significantly over the photon energy range of the proposed measurements. We present in Fig. 13 a representative illustration of the data acquisition considerations. In each panel the vertical green dashed lines indicate the limits of the Blowfish acceptance. The top panel shows the theoretical asymmetry based on the calculations of Schmitt and Arenhövel [10]. The second panel shows the cross section (including polarization contributions). The third panel shows the "Figure of Merit" for such an asymmetry measurement (in black) and the approximate acceptance of the Blowfish in its HIFROST configuration. Fig. 14 shows the HIFROST and the Blowfish. The HIFROST is necessarily inserted at 90^o to the axis of symmetry of the Blowfish due to the limitation of the length of the HIFROST fridge. This changes the otherwise ϕ-symmetry of the Blowfish as well as its θ-symmetry. The result is shown here in blue. A qualitative illustration of the statistical precision of the data to be obtained is best illustrated in the lowest panel by the product of the figure of merit and the acceptance. By comparing the uppermost and lowest panels we see that the acceptance of the Blowfish in this configuration is very well matched to the expected data; the statistically most precise data will be obtained where the measurements are most sensitive to the tensor analyzing power we are measuring.

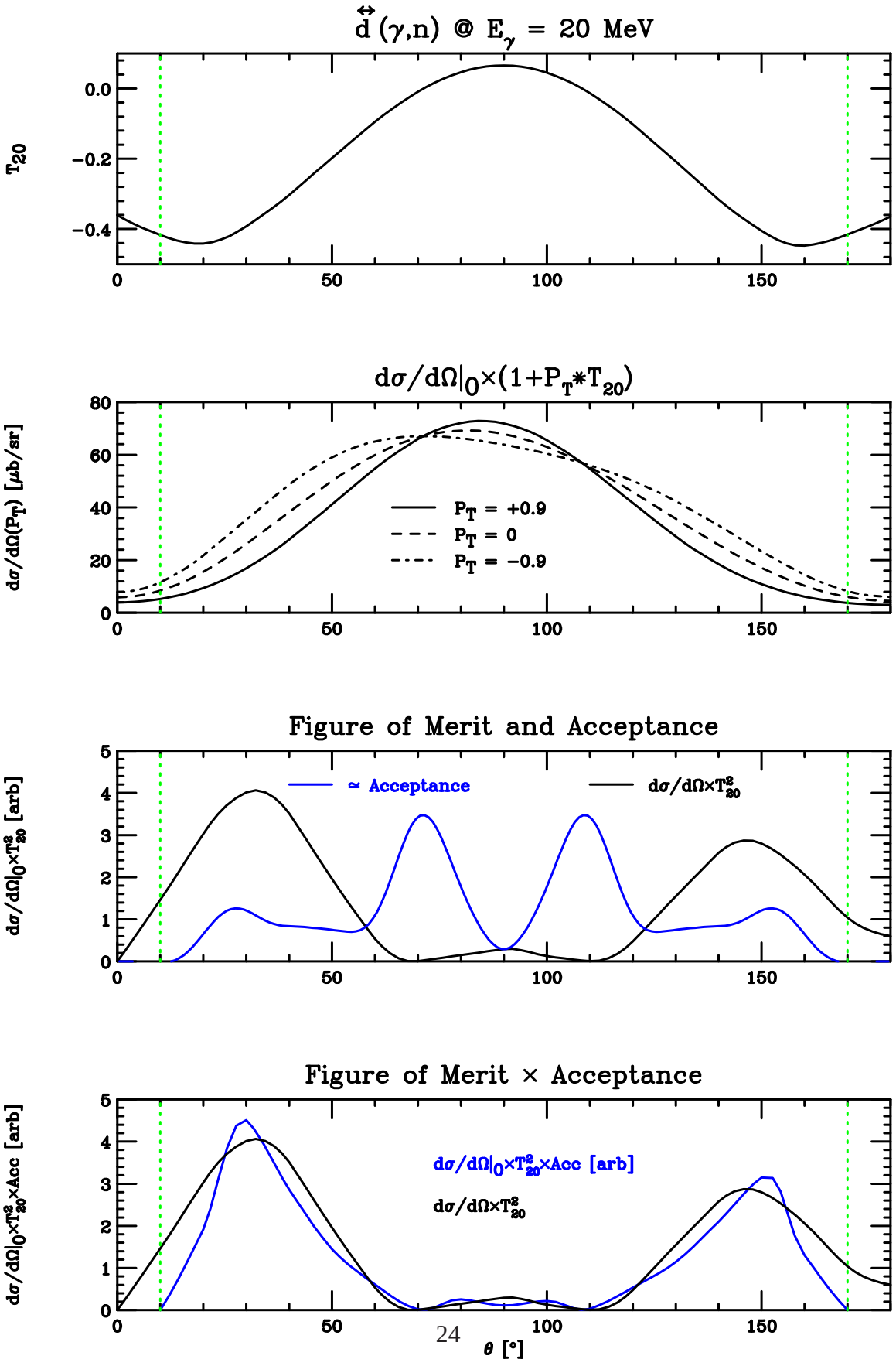

Figure 13: Considerations for data acquisition. See text for explanations of curves.

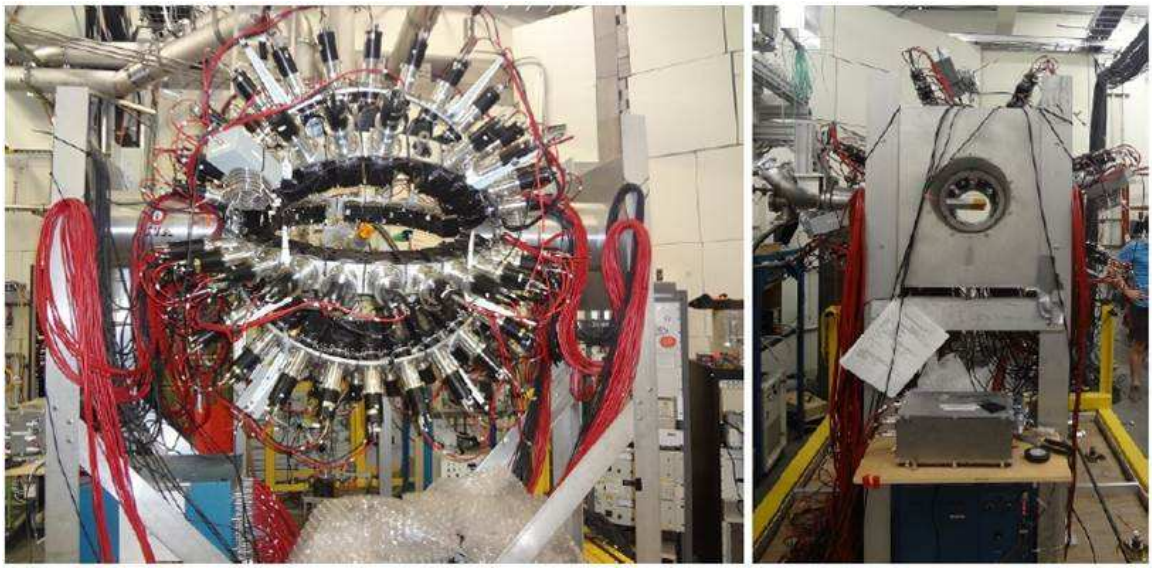

Figure 14: The HIFROST in place inside the Blowfish. The left frame shows a head-on view; the right frame shows a side view. The orange section at the end of the HIFROST fridge is the region in which the polarized target material is located.

5 Summary

We are proposing a measurement of the tensor analyzing power in the reaction $\overleftrightarrow{d}\ (\gamma, n)p$ in the photon energy range $4\ MeV\ \leq\ E_\gamma\ \leq\ 20\ MeV$. The measurements will use the polarized target system currently being installed, with the addition of a second microwave system to generate the purely tensor polarization, and the $Blowfish$ detector . It will be the first nuclear physics measurement using such a target. These high precision measurements will place tight constraints on current theories of deuteron structure and shed light on discrepancies observed between some data and current theoretical calculations.

The beam time requested represents 17 days of running assuming two-shift operation. Most of the overhead activities required will be performed during the night shift when no beam is available, making for a very efficient run.

References

[1] F. Smit and F. Brooks, Nucl. Phys. **A465**, 429 (1987).

[2] B. Sawatzky, PhD. Dissertation, University of Virginia, 2005.

[3] M. Blackston *et al.*, Phys. Rev. **C78**, 034003 (2008).

[4] S. Kucuker, PhD. Dissertation, University of Virginia, 2011.

[5] D. Skopik *et al.*, Phys. Rev. **C9**, 531 (1974).

[6] G. Pribham, MSc. Thesis, University of Saskatchewan, 2014.

[7] A. D. Graeve *et al.*, Phys. Rev. **C45**, 860 (1992).

[8] R. Nath *et al.*, Nucl. Phys. **A194**, 49 (1972).

[9] H. Arenhoevel, Few-Body Systems **4**, 55 (1988).

[10] K.-M. Schmitt and H. Arenhoevel, Few-Body Syst. **7**, 95 (1989).

[11] P. von Neumann *et al.*, Phys. Rev. Lett. **88**, 202304 (2002).

[12] S. Christlmeier and H. Griesshammer, Phys. Rev. **C77**, 064001 (2008).

[13] L. Fil'kov *et al.*, Phys. Rev. **C61**, 044004 (2000).

[14] A. Cichocki, PhD. Dissertation, University of Virginia, 2003.

[15] I. Rachek *et al.*, Phys. Lett. **5**, 98 (2007).

[16] M. Levchuck, Few-Body Syst. **19**, 77 (1995).

[17] M. Schwamb and H. Arenhoevel, Nucl. Phys. **A 696**, 556 (2001).

[18] W. Meyer *et al.*, Nucl. Instrum. Meth. **A244**, 574 (1986).

[19] J. Carlson and R. Schiavilla, Rev. Mod. Phys. **70**, 743 (1998).

[20] J. L. Forest *et al.*, Phys. Rev. **C54**, 646 (1996).

[21] W. de Boer, Cern Report CERN-74-11 (1974).

[22] P. Hautle, PhD. Thesis.

[23] P. Hautle *et al.*, Nucl. Instrum. Meth. **A356**, 108 (1995).

[24] W. Meyer and E. Schilling, BONN-HE-85-06, C84-09-03.1 (1985).